Two-Color Pump-Probe Measurement of Photonic Quantum Correlations Mediated by a Single Phonon

Mitchell D. Anderson, Santiago Tarrago Velez, Kilian Seibold, Hugo Flayac, Vincenzo Savona, Nicolas Sangouard, and Christophe Galland

Phys. Rev. Lett. **120**, 233601 — Published 5 June 2018

DOI: 10.1103/PhysRevLett.120.233601

Two-Color Pump-Probe Measurement of Photonic Quantum Correlations Mediated by a Single Phonon

Mitchell D. Anderson[†],[1] Santiago Tarrago Velez[†],[1] Kilian Seibold,[1] Hugo Flayac,[1] Vincenzo Savona,[1] Nicolas Sangouard,[2] and Christophe Galland[1]

[1] *Institute of Physics, Ecole Polytechnique Fédérale de Lausanne (EPFL), CH-1015 Lausanne, Switzerland*
[2] *Departement Physik, Universität Basel, Klingelbergstrasse 82, CH-4056 Basel, Switzerland*

(Dated: May 4, 2018)

We propose and demonstrate a versatile technique to measure the lifetime of the one-phonon Fock state using two-color pump-probe Raman scattering and spectrally-resolved, time-correlated photon counting. Following pulsed laser excitation, the $n = 1$ phonon Fock state is probabilistically prepared by projective measurement of a single Stokes photon. The detection of an anti-Stokes photon generated by a second, time-delayed laser pulse probes the phonon population with sub-picosecond time resolution. We observe strongly non-classical Stokes–anti-Stokes correlations, whose decay maps the single phonon dynamics. Our scheme can be applied to any Raman-active vibrational mode. It can be modified to measure the lifetime of $n \geq 1$ Fock states or the phonon quantum coherences through the preparation and detection of two-mode entangled vibrational states.

PACS numbers:

Introduction — Phonons, the quantized excitations of internal vibrational modes in crystals and molecules, span a broad frequency range up to ~ 100 THz. At these high frequencies, thermal occupancy at room temperature is much less than one, so that quantum effects are readily observable. For example, creation and annihilation of a single phonon within one short laser pulse produces non-classically correlated Stokes–anti-Stokes (SaS) photon pairs [1–3], as observed in pulsed Raman scattering from a diamond crystal [4], liquid water [5] and other molecular species [6]. With the advent of quantum optomechanics, the quantisation of lower frequency (MHz to GHz) mechanical oscillations was also evidenced in several experiments using phase sentive detection [7, 8] and photon counting [9, 10]. Finally, in a series of recent experiments, Raman-active phonon modes in pure diamond [11–16] and gaseous hydrogen [17–19] have been used to store and process classical and quantum information on picoseconds time scales at room-temperature. Developing versatile schemes and techniques to address non-classical phonon states in bulk and nanoscale systems is thus a promising research direction to improve our understanding of quantum effects occurring at ambient conditions and leverage them for quantum technologies.

In this Letter, we present a new scheme to measure the creation and annihilation of a single phonon Fock state with sub-picosecond time resolution (Fig. 1), which can be applied on any Raman-active high frequency mode, such as ubiquitously found in organic materials. Our scheme is conceptually similar to the one recently applied to an optomechanical cavity with a GHz mechanical oscillator [9], although we don't use any optical cavity and measure the dynamics on time scales that are 5 to 6 orders of magnitude shorter. We use diamond in a proof-of-principle experiment (phonon frequency $\Omega_m/2\pi = 39.9$ THz), but in contrast to Refs. [11–19], our scheme does not rely on the polarization selection rule of Raman scattering to temporally distinguish between photons. It is therefore not restricted to diamond and can be applied to low-dimensional structures and molecules as well, in the solid, liquid or gaseous phase. Indeed, we use two-color excitation and spectral multiplexing to distinguish the photons from the *write* and *read* steps. In the *write* step, a laser pulse centered at frequency ω_1 leads to Stokes scattering with low probability $p_S \ll 1$ (two-phonon generation occurs with probability $\propto p_S^2 \ll p_S$). Detection of a Stokes (S) photon at frequency $\omega_1 - \Omega_m$ projects the phonon onto the Fock state $|n = 1\rangle$. In the *read* step, after a controllable time delay Δt, a second synchronised pulse centered at a different frequency ω_2 is used to probe the population of the conditional phonon Fock state by detection of an anti-Stokes (aS) photon at frequency $\omega_2 + \Omega_m$. The value of the second-order cross-correlation $g^{(2)}_{S,aS}(\Delta t)$ between

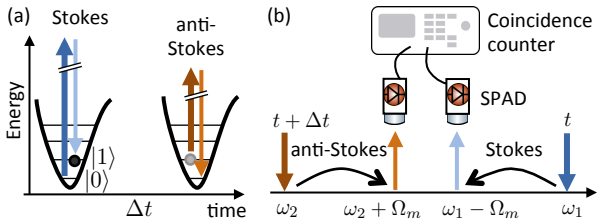

FIG. 1: (a) Concept of the experiment: The first (write) laser pulse probabilistically prepares the phonon in state $|n = 1\rangle$ upon detection of a Stokes photon. The second (read) pulse, after a time delay Δt, converts this phonon into an anti-Stokes photon. (b) Schematics of the photon counting in the frequency domain (SPAD: single-photon avalanche photodiode). The choice of ω_1 and ω_2 is completely free, as long as the Stokes and anti-Stokes photons can be efficiently isolated by spectral filtering.

the S and aS photons witnesses the non-classical nature of the two-photon state produced by the exchange of a single phonon [20] (see SM, Sec. 1, [21] for a more general discussion). The dynamics of this non-classical SaS correlation can be tracked by scanning Δt, revealing the single-phonon lifetime.

Experimental Setup — Our experimental setup is depicted in Fig. 2. The two synchronized femtosecond pulse trains are generated by a Ti:Sapph oscillator (Tsunami, Spectra Physics, 80 MHz repetition rate) and a frequency-doubled optical parametric oscillator (OPO-X fs, APE Berlin). We can independently tune the Ti:Sapph wavelength between 740 and 860 nm and the OPO wavelength between 505 and 740 [22]. The OPO generates the write pulse, while the Ti:Sapph is sent through a delay line to provide the read pulse. The read and write pulses are combined at a dichroic mirror before being focused on a synthetic diamond crystal (~ 300 μm thick) cut along the 1-0-0 crystal axis. We use tunable interference filters (highlighted in green in Fig. 2) to block the spectral components of the excitation pulses that overlap with the detection window. The sample is studied in transmission with a pair of objective lenses in order to fulfill momentum conversation in the exchange of the same phonon in the read and write scattering processes. After the sample, we block most of the laser light with a combination of tunable short and long pass filters, and send the signal either to a spectrometer equipped with a cooled CCD array or to a single mode fiber, which selects a single spatial mode of the photons. Since momentum is conserved during Raman scattering, this allows us to probe a well-defined phonon spatial mode in the bulk crystal. After the fiber, light is collimated and sent to a tunable dichroic mirror (TuneCube, AHF analysentechnik AG), which allows us to separate the S and aS photons, depending on their wavelengths, by rotating a tunable filter (here a long-pass). The separated signals are further spectrally filtered before impinging on fiber-coupled single photon avalanche photodiodes (SPADs) connected to a coincidence counter.

Results — In each experiment, we begin by tuning the Ti:Sapph and OPO to center frequencies $\tilde{\omega}_2$ and $\tilde{\omega}_1$ so that $\tilde{\omega}_1 - \tilde{\omega}_2 = \Omega_m$. When the two pulses overlap, both spatially and temporally, strong coherent anti-Stokes Raman scattering (CARS) at frequency $\tilde{\omega}_1 + \Omega_m$ is generated. We use this signal to find the zero time delay and optimize the spatial overlap of the two excitation beams.

The center frequency of the write pulse is then tuned so that the S and aS peaks are spectrally separated from the read and write pulses. As a first demonstration, the central wavelengths of the write and read pulses are set to 696 nm and 810 nm, respectively. This results in S photons at 767 nm (1.619 eV) and aS photons at 732 nm (1.695 eV), as seen on the Raman spectrum of Fig. 3a, inset. Figure 3a presents the coincidence histogram obtained at zero write-read delay in this configuration. The

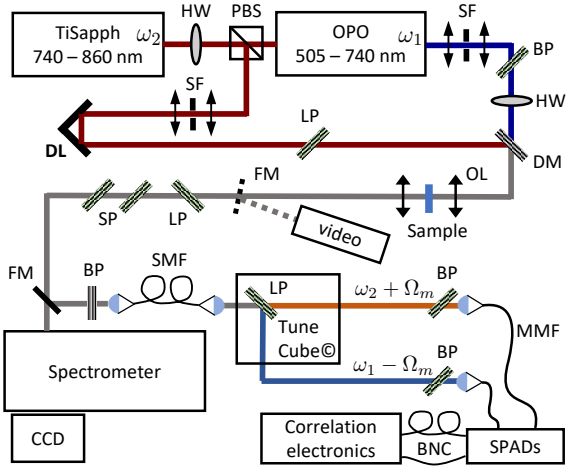

FIG. 2: Schematic drawing of the experimental setup. HW: half-wave plate; PBS: polarizing beam-splitter; SF: spatial filter; SP/LP/BP: short/long/band-pass filters (tunable filters are highlighted in green); DL: delay line; DM: Dichroic mirror; OL: objective lens (numerical aperture = 0.8); SMF: single-mode fiber (HP780, Thorlabs); MMF: graded index multimode fiber (100 μm core, NA 0.29, OZ Optics); FM: flip mirror. A video camera is used to overlap the beams.

$t = 0$ ns peak corresponds to events where one photon is detected in each channel within the same write-read pulse sequence. Since the delay between two repetitions (12.5 ns) is three to four orders of magnitude longer than the phonon lifetime, the side peaks are due to uncorrelated photons ("accidental" coincidences). The number of coincidences in the central peak, divided by the average number of coincidences in the side peaks, is a measure of $g^{(2)}_{S,aS}(0)$, the normalized second-order cross-correlation function between the S photons produced in the write pulse and the aS photons produced in the read pulse [9, 23].

The Cauchy-Schwartz inequality sets an upper bound on the possible value of the cross-correlation for classical fields $g^{(2)}_{S,aS}(0) \leqslant \left(g^{(2)}_{S,S}(0) g^{(2)}_{aS,aS}(0)\right)^{1/2}$, where the terms on the RHS are the second-order auto-correlation functions of the S and aS fields [24, 25]. We expect that $g^{(2)}_{S,S}(0) = 2$ since the spontaneously emitted S photons follow the same (thermal) statistics as in parametric down-conversion below threshold (See SM, Sec. 1-2). However, this is true only in the single-mode situation, as the the Stokes auto-correlation function falls as $1 + 1/N$ with N the number of phonon and photon modes (see SM, Sec. 1-2). We therefore used a 50/50 beam splitting fiber to measure the auto-correlation of the S channel and found $g^{(2)}_{S,S}(0) = 2 \pm 0.1$ (see Fig. S1), confirming that our experiment measures the state of a single phonon mode. Although the count rate on the aS detector was not sufficient to measure precisely $g^{(2)}_{aS,aS}(0)$, we cannot think of any reason why it should be larger

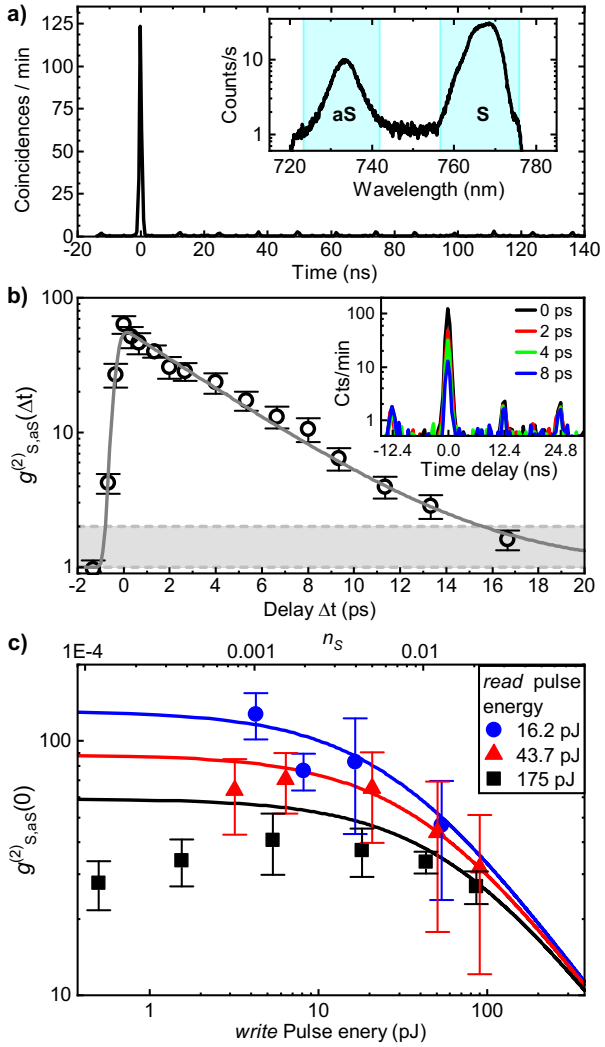

FIG. 3: (a) S–aS coincidence histogram (20 min integration). The S (resp. aS) count rates were $< 2.5 \cdot 10^4$ Hz (resp. $< 8 \cdot 10^2$ Hz), with a dark count rate $< 5 \cdot 10^2$ Hz. The OPO (resp. TiSapph) powers just after the sample were ~ 1.5 mW (resp. ~ 3.5 mW). Inset: representative Raman spectrum; the pass-bands of the filters placed before the S and aS detectors are overlaid in blue. (b) *Write-read* delay dependence of the measured S–aS correlation (open circles) and fit (dashed line) using an exponential decay (time constant = 3.9±0.7 ps) convoluted with the instrument response (Gaussian with standard deviation $\sigma = 223$ fs, see SM). The gray area marks the classical bounds. Inset: coincidence histograms at different delays. (c) Measured SaS correlations at zero delay vs. average power in the *write* beam (symbols) for different powers in the *readout* beam. Solid lines are the result of the simplified analytical model presented in the SM Sec. 4. It has two free parameters: the overall collection and detection efficiency η (probability of registering a S or aS photon emitted in the right spatial mode) and a factor α accounting for the non-ideal phonon-photon conversion in the read pulse, which we relate to imperfect mode overlap. The best fit to the data is obtained with $\eta = 0.07$ and $\alpha = 0.3$.

than 2 since the aS photons should carry the thermal statistics of the phonon mode. In summary, the classical bound to our measurement is $g^{(2)}_{S,aS}(0) \leqslant 2$. The measured value $g^{(2)}_{S,aS}(0) = 63.4 \pm 9.7$ in Fig. 3a,b thus violates the Cauchy-Schwartz inequality by 6 standard deviations and is a proof of quantum correlations between the S and aS photons, mediated by the exchange of a single phonon.

We then repeat the coincidence measurement for many different positions of the delay line and obtain the time dependent correlation function $g^{(2)}_{S,aS}(\Delta t)$ (Fig. 3b). The correlations decay with a $1/e$ time constant of 3.9 ± 0.7 ps (bounds for 95% confidence), in agreement with the literature values of the optical phonon lifetime in diamond [11, 26]. This demonstrates that we are able to measure the lifetime of a phonon Fock state by following the decay of non-classical S–aS correlations.

In order to understand what determines the precise value of $g^{(2)}_{S,aS}$ and what limits the achievable degree of non-classical correlations, we study the dependence of the zero-delay correlation $g^{(2)}_{S,aS}(0)$ on the powers in the write (P_w) and read (P_r) beams (Fig. 3c) and compare the results to an analytically soluble quantum model of parametrically coupled photon-phonon modes at zero temperature (SM, Sec. 2). In direct analogy with the physics of photon pairs produced by parametric down-conversion (see also SM, Sec. 1) [27], we find that $g^{(2)}_{S,aS}(0)$ decreases as $1/n_S \propto 1/P_w$ where n_S is the average S photon number produced by the write pulse. This can be understood as the consequence of the growing probability of exciting the $|n = 2\rangle$ phonon Fock state at higher power compounded with the fact that our detectors cannot resolve the photon number.

Interestingly, at low P_w the correlation saturates at a value that depends on the power in the read pulse P_r. We can explain this behavior by the noise generated in the read pulse, which has three components. (i) The thermal phonons (thermal occupancy $n_{th} < 2 \cdot 10^{-3}$) are responsible for uncorrelated aS emission. If this were the only source of noise, then $g^{(2)}_{S,aS}(0) \to 1/n_{th}$ at low write powers P_w, irrespective of the read power P_r. (ii) Yet, another intrinsic noise source related to the Raman process is SaS pair emission in the read pulse [2], which scales quadratically with P_r. (iii) Finally, we identified spontaneous four-wave mixing (SM) as another source of uncorrelated counts on the aS detector in the read pulse. In the SM, Sec. 3, we present a more complete quantum model in which the effects (i-iii) are accounted for. Its dynamics is solved numerically at non-zero temperature and the results reproduce qualitatively well our observations without fitting parameters, suggesting that we have a comprehensive understanding of the noise sources limiting the value of $g^{(2)}_{S,aS}(0)$.

The simplified model used to fit the data in Fig. 3c can also be used to compute the expected second-order autocorrelation of the aS photons $g^{(2,cond)}_{aS,aS}(0)$ conditional on

the detection of a S photon in the write pulse, as would be measured to characterize heralded single-photons [23] (see SM). We find values of $g^{(2,cond)}_{aS,aS}(0)$ well below 0.1 for the parameters corresponding to most data points of Fig. 3c, demonstrating that our experiment indeed probes the dynamics of the $|n=1\rangle$ phonon Fock state, with negligible contribution of $n \geqslant 2$ eigenstates.

A route to increase the measured quantum correlation toward the $1/n_{th}$ thermal limit is the use of a cavity in the resolved sideband regime to select only S and aS processes in the write and read pulses, respectively [23]. This is where the broad tunability of our setup would become particularly relevant.

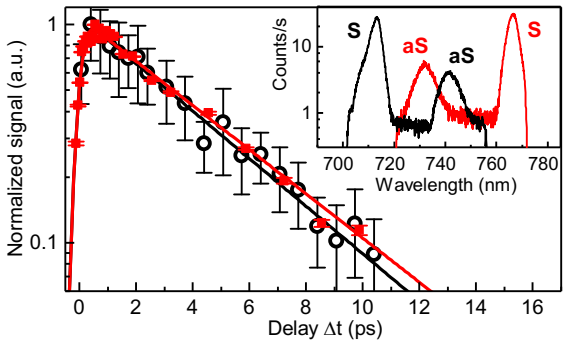

FIG. 4: a) Decay of the normalized SaS correlation $(g^{(2)}_{S,aS}(\Delta t) - 1)/(g^{(2)}_{S,aS}(0) - 1))$ (symbols) as a function of write–read delay Δt for two configurations of laser wavelengths (red and black colors), yielding S and aS peaks as shown in the inset. The fitted exponential decays (solid lines) have time constants 4.2 ± 0.5 ps (red line) and 4.0 ± 0.3 ps (black line).

Indeed, we show in Fig. 4 that we can perform this measurement using different configurations of the excitation/detection wavelengths accessible with our instruments. For example, the write and read pulses were also set at 650 nm and 821 nm, respectively, yielding S and aS photons at 712 nm (1.74 eV) and 740 nm (1.67 eV) (see Fig. 4, inset). Although the absolute value of $g^{(2)}_{S,aS}(0)$ depends on the laser powers, on the quality of alignment and beams' overlap, on the amount of cross-talk between the S and aS channel and on the amount of background emission, after normalization both data sets accurately track the phonon dynamics. This demonstrates the broad tunability of our setup (limited here by the available filters) and the robustness of our technique.

Conclusion — Our scheme constitutes a broadly applicable technique for the time-resolved measurement of quantum correlations mediated by high frequency vibrational modes, which can be observed even at room-temperature due to their vanishing thermal occupancy. As we verified by rotating the linear polarization of the write beam, our scheme is polarization insensitive, so that it can be applied to any Raman-active mode. It is well suited to study quantum dynamics in individual nanosystems – in principle down to a single molecule [28]. As shown in Ref. [11–19], Raman-active phonons are potential candidates for room-temperature quantum information processing. Our scheme extends the feasibility of this approach to a much broader range of material systems, which can be optimized for coupling efficiency and longer phonon lifetime.

The wide tunability of our setup will allow to leverage the resonant enhancement provided by electronic transitions or nanocavities, while spectral multiplexing and photon counting make it possible to measure cross-correlations between different normal modes (by triggering the start and stop detectors with two different Raman lines), thereby probing inter-mode coupling dynamics. Moreover, by triggering the coincidence counter upon multi-photon detection in the write step (using spatial [29, 30] or temporal [31] multiplexing or a direct photon number resolving detector [32, 33]), our technique would probe the dynamics of higher vibrational Fock states $(n > 1)$ [34]. The probabilistic nature of the scheme, however, means that the rate of successful events will drop exponentially with n. Finally, this work constitutes the basis for more advanced measurement schemes where phonon coherences are measured using vibrational two-mode entangled states [35] and photon-phonon entangled states [36]. This could lead to new ways of studying quantum phenomena in organic systems, which play essential roles in photochemistry and possibly in some biological reactions [37, 38].

Acknowledgements — We thank Pascal Gallo and Niels Quanck for providing diamond crystals; Mark Kasperczyk for helpful discussions regarding the experiment, Philippe Roelli, Nils Kipfer and Tianqi Zhu for assistance in the laboratory and Vivishek Sudhir for insightful discussion of the results. This work was made possible by the Swiss National Science Foundation (SNSF), through the grants number PP00P2-170684 and PP00P2-150579.

† M.D.A. and S.T.V. contributed equally to this work.

[1] D. N. Klyshko, Sov. J. Quantum Electron. **7**, 755 (1977).
[2] C. A. Parra-Murillo, M. F. Santos, C. H. Monken, and A. Jorio, Phys. Rev. B **93**, 125141 (2016).
[3] M. K. Schmidt, R. Esteban, A. González-Tudela, G. Giedke, and J. Aizpurua, ACS Nano **10**, 6291 (2016).
[4] M. Kasperczyk, A. Jorio, E. Neu, P. Maletinsky, and L. Novotny, Opt. Lett. **40**, 2393 (2015).
[5] M. Kasperczyk, F. S. de Aguiar Júnior, C. Rabelo, A. Saraiva, M. F. Santos, L. Novotny, and A. Jorio, Phys. Rev. Lett. **117**, 243603 (2016).
[6] A. Saraiva, F. S. d. A. Júnior, R. de Melo e Souza, A. P. Pena, C. H. Monken, M. F. Santos, B. Koiller, and A. Jorio, Phys. Rev. Lett. **119**, 193603 (2017).
[7] T. P. Purdy, K. E. Grutter, K. Srinivasan, and J. M. Taylor, Science **356**, 1265 (2017).

[8] V. Sudhir, R. Schilling, S. Fedorov, H. Schütz, D. Wilson, and T. Kippenberg, Phys. Rev. X **7**, 031055 (2017).

[9] R. Riedinger, S. Hong, R. A. Norte, J. A. Slater, J. Shang, A. G. Krause, V. Anant, M. Aspelmeyer, and S. Gröblacher, Nature **530**, 313 (2016).

[10] S. Hong, R. Riedinger, I. Marinković, A. Wallucks, S. G. Hofer, R. A. Norte, M. Aspelmeyer, and S. Gröblacher, Science **358**, 203 (2017).

[11] K. C. Lee, B. J. Sussman, M. R. Sprague, P. Michelberger, K. F. Reim, J. Nunn, N. K. Langford, P. J. Bustard, D. Jaksch, and I. A. Walmsley, Nat Photon **6**, 41 (2012).

[12] D. G. England, P. J. Bustard, J. Nunn, R. Lausten, and B. J. Sussman, Phys. Rev. Lett. **111**, 243601 (2013).

[13] D. G. England, K. Fisher, J.-P. W. MacLean, P. J. Bustard, R. Lausten, K. J. Resch, and B. J. Sussman, Phys. Rev. Lett. **114**, 053602 (2015).

[14] P.-Y. Hou, Y.-Y. Huang, X.-X. Yuan, X.-Y. Chang, C. Zu, L. He, and L.-M. Duan, Nat. Commun. **7**, 11736 (2016).

[15] K. A. G. Fisher, D. G. England, J.-P. W. MacLean, P. J. Bustard, K. J. Resch, and B. J. Sussman, Nat. Commun. **7**, 11200 (2016).

[16] K. A. G. Fisher, D. G. England, J.-P. W. MacLean, P. J. Bustard, K. Heshami, K. J. Resch, and B. J. Sussman, Phys. Rev. A **96**, 012324 (2017).

[17] P. J. Bustard, R. Lausten, D. G. England, and B. J. Sussman, Phys. Rev. Lett. **111**, 083901 (2013).

[18] P. J. Bustard, J. Erskine, D. G. England, J. Nunn, P. Hockett, R. Lausten, M. Spanner, and B. J. Sussman, Opt. Lett., OL **40**, 922 (2015).

[19] P. J. Bustard, D. G. England, K. Heshami, C. Kupchak, and B. J. Sussman, Opt. Lett., OL **41**, 5055 (2016).

[20] R. J. Glauber, Phys. Rev. **130**, 2529 (1963).

[21] See Supplemental Material [url] for a discussion on the Cauchy-Schwartz inequality (Sec. 1), details on the quantum models (Sec. 2-3) and the data analysis (Sec. 4-6), which includes Refs. [2, 24, 25, 27, 39, 40].

[22] Tuning curves available at http://www.ape-berlin.de/en.

[23] C. Galland, N. Sangouard, N. Piro, N. Gisin, and T. J. Kippenberg, Phys Rev Lett **112**, 143602 (2014).

[24] M. Reid and D. Walls, Phys. Rev. A **34**, 1260 (1986).

[25] A. Kuzmich, W. P. Bowen, A. D. Boozer, A. Boca, C. W. Chou, L.-M. Duan, and H. J. Kimble, Nature **423**, 01714 (2003).

[26] M. S. Liu, L. A. Bursill, S. Prawer, and R. Beserman, Phys. Rev. B **61**, 3391 (2000).

[27] P. Sekatski, N. Sangouard, F. Bussieres, C. Clausen, N. Gisin, and H. Zbinden, J. Phys. B At. Mol. Opt. Phys. **45**, 124016 (2012).

[28] S. Yampolsky, D. A. Fishman, S. Dey, E. Hulkko, M. Banik, E. O. Potma, and V. A. Apkarian, Nat Photon **8**, 650 (2014).

[29] A. Divochiy, F. Marsili, D. Bitauld, A. Gaggero, R. Leoni, F. Mattioli, A. Korneev, V. Seleznev, N. Kaurova, O. Minaeva, et al., Nat. Photonics **2**, nphoton.2008.51 (2008).

[30] E. A. Dauler, A. J. Kerman, B. S. Robinson, J. K. W. Yang, B. Voronov, G. Goltsman, S. A. Hamilton, and K. K. Berggren, J. Mod. Opt. **56**, 364 (2009).

[31] M. J. Fitch, B. C. Jacobs, T. B. Pittman, and J. D. Franson, Phys. Rev. A **68**, 043814 (2003).

[32] J. Kim, S. Takeuchi, Y. Yamamoto, and H. H. Hogue, Appl. Phys. Lett. **74**, 902 (1999).

[33] A. J. Miller, S. W. Nam, J. M. Martinis, and A. V. Sergienko, Appl. Phys. Lett. **83**, 791 (2003).

[34] H. Wang, M. Hofheinz, M. Ansmann, R. C. Bialczak, E. Lucero, M. Neeley, A. D. O'Connell, D. Sank, J. Wenner, A. N. Cleland, et al., Phys. Rev. Lett. **101**, 240401 (2008).

[35] H. Flayac and V. Savona, Phys. Rev. Lett. **113**, 143603 (2014).

[36] V. C. Vivoli, T. Barnea, C. Galland, and N. Sangouard, Phys. Rev. Lett. **116**, 070405 (2016).

[37] M. M. Wilde, J. M. McCracken, and A. Mizel, Proc. R. Soc. Lond. Math. Phys. Eng. Sci. **466**, 1347 (2010).

[38] E. J. O'Reilly and A. Olaya-Castro, Nat. Commun. **5**, 3012 (2014).

[39] P. Farrera, N. Maring, B. Albrecht, G. Heinze, and H. de Riedmatten, Optica, OPTICA **3**, 1019 (2016).

[40] H. Flayac, D. Gerace, and V. Savona, Sci. Rep. **5**, 11223 (2015).